Associative detachment in low energy collisions between hydrogen atoms and atomic halogen anions

M Čížek†, J Horáček†, F A U Thiel‡ and H Hotop‡§

†Department of Theoretical Physics, Faculty of Mathematics and Physics, Charles University Prague, V Holešovičkách 2, 180 00 Praha 8, Czech Republic

‡Department of Physics, University of Kaiserslautern, D-67653 Kaiserslautern, Germany

Abstract. Using an improved nonlocal resonance theory, total cross sections, rovibrational final state distributions and electron spectra for low-energy (< 2 eV) associative detachment (AD) collisions between atomic hydrogen atoms and negative halogen ions X^- (X = F, Cl, Br) as well as deuterium atoms and F^- ions have been calculated. The model involves realistic long-range interactions for the $H+X^-$ systems and takes into account the dependence of the dipole-modified threshold exponent on internuclear distance. Good agreement is found between experimental data for the total AD cross sections and the theoretical results. In the calculated electron energy spectra nonlocal effects are manifest through step structure which is (almost) independent of collision energy; this structure should therefore be observable in experiments with rather modest collision energy resolution. For illustration, electron spectra are presented which correspond to realistic experimental conditions with regard to the energy widths of the electron spectrometer and the collision energy distribution. The rovibrational final state distributions in the formed $HX(v, J)$ molecules are reported for a thermal kinetic energy distribution at $T \approx 300$ K; for HF, DF, and HCl the rotational-summed vibrational populations p_v are compared with previous theoretical and experimental results.

PACS numbers: 34.10.+x, 34.20.-b, 34.50.-s, 82.40.Dm

Submitted to: *J. Phys. B: At. Mol. Opt. Phys.*

§ To whom correspondence should be addressed

1. Introduction

In low energy collisions of atomic negative ions X^- with atoms or molecules Y the associative detachment (AD) process

$$\mathrm{Y} + X^- \to \mathrm{Y}X(v, J) + \mathrm{e}^-(\varepsilon_{vJ}) \tag{1.1}$$

represents an important loss mechanism for negative ions and an efficient source for molecule formation (when stable molecules $\mathrm{Y}X$ exist)[1, 2]. These processes are believed to proceed through temporary formation of a short-lived resonant state $(\mathrm{Y}X)^-$. Recently, a nonlocal resonance model, using the projection operator formalism, has been applied to the important AD reaction $\mathrm{H} + \mathrm{H}^- \to \mathrm{H}_2 + \mathrm{e}^-$ which is relevant for molecule formation in interstellar space [3, 4, 5]. It was shown that nonlocal effects are rather small in this system and that a local theory yields results for the total and partial, (v, J)-specific cross sections $\sigma_{vJ}(E)$ (E = relative collision energy) which are in satisfactory agreement with those of the nonlocal theory [5]. Large differences between local and nonlocal theory were found only for small v for which also the magnitude of the cross section $\sigma_{vJ}(E)$ is small and contributes negligibly to the total cross section [5]. It should be emphasised that the development of a reliable theory for AD reactions is particularly important in view of the fact that experimental results for partial cross sections $\sigma_{vJ}(E)$ are sparse and difficult to obtain. To date no electron energy spectra for AD processes in collisions of atomic negative ions with atoms (in particular Y = H) have been reported to our knowledge. Some experimental data do exist for the collision energy dependence of the *total* AD cross section in reactions of atomic hydrogen [6] and halogen anions [7] with hydrogen atoms and for some other simple diatomic systems [8, 9]. Total cross sections, however, do not represent a sensitive probe of the theoretical description, and it is therefore highly desirable to elucidate the detailed consequences of different facets of the theory through predictions of experimentally observable differences in the partial (v, J) cross sections $\sigma_{vJ}(E)$, as detectable in electron energy spectra or - as in the case of the hydrogen halides - via infrared spectroscopy [10, 11, 12].

In the present paper, we address the AD reactions of the atomic halogen anions X^- (X = F, Cl, Br) with hydrogen atoms at low collision energy (0.01 to about 1 eV). First experimental determinations of the rate coefficient k_{AD} (i.e. the collision velocity averaged product of the total AD cross section $\sigma_{\mathrm{AD}}(E)$ times the collision velocity $v(E)$, i.e. $k_{\mathrm{AD}} = \langle\sigma_{\mathrm{AD}}(E)v(E)\rangle$) for these AD reactions at thermal collision energies were obtained by Fehsenfeld *et al* [13, 14] and by Smith and Adams [15]. In a comprehensive recent crossed beams study Huels *et al* [7] investigated the collision energy dependence of the total cross section $\sigma_{\mathrm{e}}(E)$ for electron production involving all the atomic halogen anions (including I^-) for relative collision energies E over the range 0.1 to 20 eV, i.e. down to energies for which only AD occurs (as characterised in previous work [16]). The ion laboratory energies went down to typically $E_{\mathrm{L}} \approx 6$ eV, corresponding to center-of-mass collision energies E between 0.4 eV ($\mathrm{H} + \mathrm{F}^-$) down to about 0.1 eV ($\mathrm{H} + \mathrm{I}^-$) [7] at lab energy widths around 0.6 eV and ion currents of a few nA. The experimental results were found to be in satisfactory agreement with the results of simple classical model calculations for the detachment process [7]. The only experimental studies of the partial cross sections for the AD systems in question was carried out by Leone's group [10, 11, 12]. Using infrared emission spectroscopy $\mathrm{Y}X(v,J) \to \mathrm{Y}X(v-1,J\pm 1)$ of the radiation from the molecules $\mathrm{Y}X(v,J)$, as produced in the AD reaction for the systems $\mathrm{H,D}+\mathrm{F}^-$ in a flowing afterglow apparatus at $T = 300$ K, they determined the nascent vibrational state distribution of the HF and DF product molecules (due to rotational relaxation and limited optical resolution, no detailed information could be obtained on the nascent rotational distribution). For HF, good agreement was found with theoretical results of Gauyacq [17] who treated the AD process with the zero-range-potential method including nonadiabatic effects. No detailed comparison with theory was made for the DF system for which the experiment yielded a broader vibrational distribution shifted (on average) to lower energies. In this paper we treat the AD process for low energy collisions between atomic halogen anions with hydrogen atoms, using an improved nonlocal resonance model. The model involves realistic long-range interactions for the $\mathrm{H}+X^-$ systems and takes into account the dependence of the dipole-modified threshold exponent on the internuclear distance. We report total cross sections for collision energies from 0.01 to about 1-2 eV. In the calculated electron energy spectra nonlocal effects are manifest through step structure which is (almost) independent of collision energy; this structure should therefore be observable in experiments with rather modest collision energy resolution. For illustration, electron spectra are presented which correspond to realistic experimental conditions with regard to the energy widths of the electron spectrometer and the collision energy distribution.

2. Theoretical description

From a theoretical point of view associative detachment (1.1) is described as temporary formation of a short lived resonant negative ion state $(\mathrm{Y}X)^-$ followed by autodetachment through spontaneous emission of an electron. This intuitive picture can be quantified using the projection operator formalism [18]. As a result the dynamics of the process is described with the nonlocal resonant model (see [19]). The local complex potential (LCP) approximation has been introduced and often used for calculations of the cross sections for associative detachment (see e.g. [3, 20, 21]) or for the similar process of Penning ionisation [18, 22]. The LCP approximation has also been used for the description of the inverse process of reaction (1.1), i.e. dissociative electron attachment (see e.g. [23]). However, it is known, that the LCP can not describe correctly the threshold features (Wigner cusps) seen for example in $\mathrm{HF}+\mathrm{e}^-$ or $\mathrm{HBr}+\mathrm{e}^-$ collisions [24]. The LCP approximation is also known to fail to describe correctly final state (v,J)-specific cross sections for associative detachment in some cases [25]. In the past two decades the nonlocal resonant model has successfully been used for the calculation of the resonant low-energy nonelastic electron-molecule cross sections [26, 27, 28, 29, 30, 31, 32]. Recently the nonlocal resonant model has also been applied to the calculation of associative detachment processes [5, 33]. All resonant processes in low-energy electron-molecule and ion-atom scattering can thus be comprehended within the framework of a single model, based on *ab initio* data with no adjustable parameters.

Another approach which is able to describe correctly the threshold features in resonance collisions is the zero-range-potential approximation, which has previously been used for calculations of electron-molecule collisions [34, 35] and also for associative detachment [17]. The zero-range-potential approximation is used to describe the interaction of the additional electron with the rest of the system and the nuclear degrees of freedom are treated either classically or fully quantum mechanically.

2.1. Nonlocal resonance model

The detailed derivation of the nonlocal resonance model using the projection operator formalism has been given in the review on low energy electron-molecule collisions by Domcke [19]. Inclusion of the rotational degrees of freedom and an application of the nonlocal resonance model to associative detachment is described in [5, 18]. Here we give only a brief overview. Unless stated otherwise, we use atomic units.

To define the nonlocal resonance model a diabatic basis set is assumed to exist in the Hilbert space of the system with the atomic nuclei fixed in space. The basis set is assumed to consist of one discrete state $|\phi_d\rangle$ and a set of vectors $|\phi_\varepsilon\rangle$ describing the electron continuum orthogonalised to $|\phi_d\rangle$. Generalisation to more discrete states is possible [36]. If the vectors $|\phi_d\rangle$ and $|\phi_\varepsilon\rangle$ are known we can construct the discrete state potential $V_d(R)$ and the discrete-state-continuum coupling $V_{d\varepsilon}$ as the matrix elements of the electronic hamiltonian H_{el}.

$$V_d(R) \equiv \langle\phi_d|H_{el}|\phi_d\rangle, \tag{2.1}$$

$$V_{d\varepsilon}(R) \equiv \langle\phi_d|H_{el}|\phi_\varepsilon\rangle. \tag{2.2}$$

Note that $\langle\phi_\varepsilon|H_{el}|\phi_\varepsilon\rangle = V_0(R) + \varepsilon$ where $V_0(R)$ is the usual adiabatic potential for the neutral molecule HX.

In the time-independent formalism the $\mathrm{H} + X^-$ scattering process is described by a wave function $\Psi(R, r)$ (r stands for all the electronic degrees of freedom) which can be expanded into $|\phi_d\rangle$, $|\phi_\varepsilon\rangle$

$$\Psi(R, r) = \psi_d(R)\phi_d(R, r) + \int \psi_\varepsilon(R)\phi_\varepsilon(R, r)\mathrm{d}\varepsilon. \tag{2.3}$$

It is possible to show [19] that the coefficients $\psi_\varepsilon(R)$ can be eliminated from the equations of motion and the coefficient $\psi_d(R)$ fulfills the Lippmann-Schwinger equation which after partial wave expansion reads

$$|\psi_J\rangle = |\phi_J\rangle + G_J(E)[V_d + F_J(E)]|\psi_J\rangle, \tag{2.4}$$

where $|\psi_J\rangle$ are partial wave components of $\psi_d(R)$ and $G_J(E)$ are the components of the Green function for the free particle. The vector $|\phi_J\rangle$ determines the boundary condition specific for each initial channel, and for $\mathrm{H} + X^-$ collisions it is given by a spherical cylindrical Bessel function. The difference between equation (2.4) and the standard one dimensional potential scattering is the presence of the additional term $F_J(E)$ in the effective potential. This term is a nonlocal, energy dependent, and nonhermitian operator, and it is usually called the nonlocal potential. The operator $F_J(E)$ can be written in terms of the coupling $V_{d\varepsilon}$. If the quantity $V_{d\varepsilon}$ is assumed to be spherically symmetric (with regard to mutual orientation of the internuclear axis and the direction of the electron motion) the relation between these quantities is

$$\langle R|F_J(E)|R'\rangle = \int d\varepsilon V_{d\varepsilon}(R) g_J(E-\varepsilon, R, R') V^*_{d\varepsilon}(R'), \tag{2.5}$$

where

$$g_J(E) = \left(E + \frac{1}{2\mu}\frac{d^2}{dR^2} - V_0(R) - \frac{J(J+1)}{2\mu R^2} + i\eta\right)^{-1}, \tag{2.6}$$

and η is the usual positive infinitesimal. The assumption of spherical symmetry of $V_{d\varepsilon}(R)$ should not influence much the results for angularly averaged quantities like electron spectra or total cross section. Models using the same assumption were successful in the reproduction of experimental inelastic electron-molecule cross sections [5, 29, 33]. If the unique solution $|\psi_J\rangle$ of equation (2.4) is known, the cross section for the associative detachment process creating the molecule HX in the state $|\chi^v_J\rangle$ is

$$\sigma_{v,J}(E) = \frac{2\pi^2}{E}\,(2J+1)|\langle\psi_J|V_{d\varepsilon^v_J}|\chi^v_J\rangle|^2. \tag{2.7}$$

The energy of the electron released in the process is given by energy conservation $\varepsilon^v_J = E - E^v_J$, where E^v_J is the energy of the final molecule HX in the state $|\chi^v_J\rangle$. The total AD cross section can be obtained by summation of $\sigma_{v,J}(E)$ over all accessible states (including their multiplicities) or from the relation

$$\sigma_{\mathrm{AD}}(E) = \frac{2\pi^2}{E}\sum_J (2J+1)\langle\psi_J|\frac{\mathrm{i}}{2\pi}\left(F_J - F^+_J\right)|\psi_J\rangle, \tag{2.8}$$

where F^+_J represents the adjoint operator to F_J. The electron spectrum for collision energy E can be written in terms of the cross sections (2.7)

$$\frac{\mathrm{d}\sigma}{\mathrm{d}\varepsilon}(\varepsilon, E) = \sum_{J,v}\sigma_{v,J}(E)\;\delta(\varepsilon - E + E^v_J), \tag{2.9}$$

where the sum is performed over all open channels ($E^v_J < E$). For a beam experiment, the collision energy distribution $f(E)$ has to be taken into account and the electron spectrum reads

$$\begin{aligned}\frac{\mathrm{d}\sigma}{\mathrm{d}\varepsilon}(\varepsilon) &= \int f(E)\frac{\mathrm{d}\sigma}{\mathrm{d}\varepsilon}(\varepsilon, E)\mathrm{d}E = \\ &= \sum_{J,v}\sigma_{v,J}(\varepsilon + E^v_J)\; f(\varepsilon + E^v_J).\end{aligned} \tag{2.10}$$

The sum is performed over those J,v for which $\varepsilon + E^v_J > 0$. Note that the energy scale has been chosen in such a way that the asymptotic energy of $\mathrm{H} + X^-$ is zero, i.e. the total energy of the system E gives also the relative collision energy E_{rel} of $\mathrm{H} + X^-$ in the center of mass system, adressed in section 2.3

For the calculation of the AD cross sections using the nonlocal resonance model, we have to specify three functions $V_0(R)$, $V_d(R)$ and $V_{d\varepsilon}(R)$. These functions can be constructed either directly [37, 38] calculating the matrix elements (2.1) and (2.2) or from the fit of published data for electron-molecule scattering using formulae for the resonant phase shift in terms of V_d and $V_{d\varepsilon}$. The nonlocal resonance models for $\mathrm{H}+\mathrm{Cl}^-$ and $\mathrm{H}+\mathrm{Br}^-$ have already been described in detail elsewhere [33, 39]. The potential energy curves are shown in figures 1–3. For both systems the potential $V_d(R)$ and the coupling $V_{d\varepsilon}(R)$ were constructed from the fit of eigenphases for electron-molecule scattering at distances R near the equilibrium separation of the neutral molecules. For the construction of $V_d(R)$ at distances $R > 3\ a_0$ ($a_0 = 52.9177$ pm) accurate *ab initio* data for the $\mathrm{H}X^-$potentials were used.

For the construction of the nonlocal resonance model for low-energy $\mathrm{H}+\mathrm{F}^-$ collisions we collected *ab initio* data from two papers. Gallup *et al* [32] constructed a nonlocal resonance model for $\mathrm{HF} + \mathrm{e}^-$ directly from their calculations of electron-molecule scattering in the fixed-nuclei limit and then they used the model for calculations of the dissociative attachment process $\mathrm{HF}+\mathrm{e}^- \to \mathrm{H}+\mathrm{F}^-$. Their model cannot be directly applied to associative detachment calculations since their discrete-state potential V_d does not exhibit the correct polarization behaviour for large R, which influences the AD cross section for small energies significantly. We therefore adjusted V_d for $R > 2.0\ a_0$ in order to get agreement with recent coupled clusters calculations of Piecuch [40] for the HF^- potential, which was the other source of *ab initio* data for our model. The procedure of adjusting $V_d(R)$ with respect to the *ab initio* data for the negative ion potential has been described in [5, 33]. Note that the energy shift due to the interaction with the continuum has been taken into account.

2.2. Local complex potential approximation

One of the goals of this paper was to find effects of the nonlocality of the resonance dynamics of the AD process on directly observable quantities. We therefore constructed a local complex potential (LCP) approximation for HCl and HBr systems. The LCP approximation is based on the replacement of the nonlocal potential $F_J(E,R,R')$ with the local quantity (see e.g. [19] or [18] for more details on the LCP approximation)

$$F_J(E,R,R') \approx \delta(R-R')[\Delta(R) - \frac{i}{2}\Gamma(R)]. \tag{2.11}$$

The local level shift $\Delta(R)$ and width $\Gamma(R)$ can be defined within the nonlocal resonance model [19]

$$V_{\mathrm{i}}(R) \equiv V_d(R) + \Delta(R) = V_0(R) + E_{\mathrm{res}}(R), \tag{2.12}$$

$$\Gamma(R)\ = \Gamma(E_{\mathrm{res}}, R), \tag{2.13}$$

where $E_{\mathrm{res}}(R)$ is the solution of the equation

$$E_{\mathrm{res}}(R) = V_d(R) - V_0(R) + \Delta(E_{\mathrm{res}}(R), R), \tag{2.14}$$

and the energy dependent level shift $\Delta(\varepsilon, R)$ and the width $\Gamma(\varepsilon, R)$ are defined in terms of $V_{d\varepsilon}(R)$

$$\Gamma(\varepsilon, R)\ \equiv 2\pi V_{d\varepsilon}(R)V^*_{d\varepsilon}(R), \tag{2.15}$$

$$\Delta(\varepsilon, R) \equiv \frac{1}{2\pi} P \int \frac{\Gamma(\varepsilon', R)}{\varepsilon - \varepsilon'} \mathrm{d}\varepsilon. \tag{2.16}$$

The local potential $V_{\mathrm{l}}(R) = V_d(R) + \Delta(R)$ gives the energy of $(\mathrm{HCl})^-$ state in the fixed nuclei limit and it is depicted in figure 1 (dashed line) together with $V_0(R)$ and $V_d(R)$ (solid lines). If the neutral molecule possesses a dipole moment the solution of the equation (2.14) is not always unique and $V_{\mathrm{l}}(R)$ is not a single-valued function near the crossing of $V_{\mathrm{l}}(R)$ and $V_0(R)$. To avoid this problem we constructed the potential $V_{\mathrm{loc}}(R)$ which follows the curve $V_{\mathrm{l}}(R)$ except near the crossing where $V_{\mathrm{loc}}(R)$ is smooth. The function $V_{\mathrm{loc}}(R)$ is shown in figures 1 and 3 as the thin solid line. Relation (2.12) yields $E_{\mathrm{res}}(R) = V_{\mathrm{l}}(R) - V_0(R)$. Replacing $V_{\mathrm{l}}(R)$ with $V_{\mathrm{loc}}(R)$ we can define in analogy with (2.13)

$$\Gamma_{\mathrm{loc}}(R) = \Gamma(V_{\mathrm{loc}}(R) - V_0(R), R). \tag{2.17}$$

To obtain the AD cross section within the LCP approximation equation (2.4) has to be solved with $V_d + F_J$ replaced by $V_{\mathrm{loc}}(R) - \frac{i}{2}\Gamma_{\mathrm{loc}}(R)$ and the solution substituted into (2.7). In addition, a further approximation is often introduced. Based on stationary phase arguments it is possible to show that

$$\langle \psi_J | V_{d\varepsilon_J^v} | \chi_J^v \rangle \simeq \langle \psi_J | \sqrt{\Gamma(R)/2\pi} | \chi_J^v \rangle, \tag{2.18}$$

i.e. $V_{d\varepsilon_J^v}(R)$ in (2.7) can be replaced by $\sqrt{\Gamma_{\mathrm{loc}}(R)/2\pi}$. Since we have full information on the dependence of $V_{d\varepsilon}$ on electron energy ε within our nonlocal resonance model it is not necessary to introduce this additional approximation in our case.

2.3. Simulation of experimental conditions

In order to calculate electron spectra which reflect realistic experimental conditions, one has to know the collision energy distribution of the investigated collision complex. The velocity distribution of a thermal hydrogen beam can be expressed by a Maxwell-Boltzmann distribution

$$F_{\mathrm{H}}^v(v) = 4 \left(\frac{m}{2k_BT} \right)^{3/2} \pi^{-1/2} \, v^2 \, \exp\left(\frac{-mv^2}{2k_BT} \right), \tag{2.19}$$

with Boltzmann constant k_B, hydrogen mass m and temperature T of the thermal ensemble. The energy distribution of the negative halogen ion-beam is assumed to be of Gaussian shape and can thus be written as

$$F_{\mathrm{X}^-}^E(E) = \left(\frac{4\ln(2)}{\pi} \right)^{1/2} \Delta E_0^{-1} \, \exp\left(-4\ln(2) \left(\frac{E - E_0}{\Delta E_0} \right)^2 \right). \tag{2.20}$$

E_0 is the average kinetic energy of the ions and ΔE_0 is the energy width defined as the full width at half maximum (FWHM). In order to calculate the relative velocity distribution of the collisional complex one has to know the velocity distribution of both collision partners. For the halogen ion-beam the velocity distribution can be obtained from $F_{\mathrm{X}^-}^E(E)$ by using the relation $F_{\mathrm{X}^-}^v(v)\,\mathrm{d}v = F_{\mathrm{X}^-}^E\left(\frac{mv^2}{2}\right)\, mv\,\mathrm{d}v$.

When the two atomic beams with $F^v_{\rm H}(v_{\rm H})$ and $F^v_{{\rm X}-}(v_{{\rm X}^-})$ collide under a laboratory collision angle $\theta_{\rm L}$ (see figure 4), the distribution of the relative velocity $v_{\rm rel}$ in the center of mass system can be calculated using the equation:

$$F^v(v_{\rm rel},\theta_{\rm L}) = \int_0^{\pi-\theta_{\rm L}} \frac{v_{\rm rel}}{\sin(\theta_{\rm L})}\, F^v_{{\rm X}^-}\left(v_{\rm rel}\cdot\left(\frac{\sin(\alpha)}{\tan(\theta_{\rm L})}+\cos(\alpha)\right)\right)\, F^v_{\rm H}\left(v_{\rm rel}\,\frac{\sin(\alpha)}{\sin(\theta_{\rm L})}\right)\,{\rm d}\alpha \tag{2.21}$$

α denotes the integration variable which accounts for the variation of $v_{\rm H}$ and $v_{{\rm X}^-}$ according to $F^v_{\rm H}$ and $F^v_{{\rm X}^-}$, respectively. The term $v_{\rm rel}/\sin(\theta_{\rm L})$ as well as the arguments of $F^v_{{\rm X}^-}$ and $F^v_{\rm H}$ in equation (2.21) are due to the variable transformation $(v_{{\rm X}^-}, v_{\rm H}) \to (v_{\rm rel}, \alpha)$. If we now consider an effusive hydrogen source, which emits into the forward direction with a $\cos(\vartheta)$ intensity distribution, the relative velocity distribution becomes

$$F^v_*(v_{\rm rel},\theta_{\rm L},\vartheta) = \frac{1}{\Omega}\int_0^{2\vartheta} F^v(v_{\rm rel},\theta_{\rm L}-\vartheta+\varphi)\ \cos(\varphi-\vartheta)\ {\rm d}\varphi, \tag{2.22}$$

when only collision angles within $\theta_{\rm L}\pm\vartheta$ are taken into account. Ω is the normalization factor given by $\Omega = \int_{-\vartheta}^{\vartheta}\ \cos(\vartheta)\ d\vartheta$. The final collision energy distribution is calculated from

$$F^E_*(E_{\rm rel},\theta_{\rm L},\vartheta) = \frac{F^v_*\ \left(\sqrt{\frac{2E_{\rm rel}}{\mu}},\theta_{\rm L},\vartheta\right)}{\mu\ \sqrt{\frac{2E_{\rm rel}}{\mu}}} \equiv f(E), \tag{2.23}$$

where the relative collision energy is given by $E_{\rm rel} = \frac{1}{2}\ \mu v^2_{\rm rel}$ and μ is the reduced mass of the collision system. Previous experiments described in the literature (especially [7]) have shown that it is rather difficult to produce negative ion-beams at low kinetic energies. Realistic ion-beam parameters are $E_0 = 5$ eV and $\Delta E_0 = 0.5$ eV [7] . Thus, these values have been used to calculate the collision energy distributions of the halogen ion-beams. For the hydrogen source a thermal ensemble with $T = 300$ K has been used. With the described procedure the relative collision energy distributions depicted in figure 4 have been calculated using the experimentally favourable and realistic values $\theta_{\rm L} = 60°$ and $\vartheta = 10°$.

We note that for a proper comparison with experimental data an average over rate coefficients k (i.e. product of relevant cross section times collision velocity $v_{\rm rel}$) should be carried out (see also the thermal average, equation (3.5)). Correspondingly the average over ${\rm d}\sigma/{\rm d}\varepsilon(\varepsilon,E)$ in equation (2.10) should be replaced by the average over $v_{\rm rel}\cdot{\rm d}\sigma/{\rm d}\varepsilon(\varepsilon,E)\equiv{\rm d}k/{\rm d}\varepsilon(\varepsilon,E)$, thus yielding instead of ${\rm d}\sigma/{\rm d}\varepsilon(\varepsilon)$ in (2.10) the quantity ${\rm d}k/{\rm d}\varepsilon(\varepsilon)$. For the adopted collision energy distribution functions (figure 4), the shapes of the resulting electron energy distributions are very similar for the two different types of averaging, and we have chosen to only show the quantities ${\rm d}\sigma/{\rm d}\varepsilon(\varepsilon)$.

3. Discussion of the results

To find the AD cross sections using the formulae (2.7-2.10) we solved the Lippmann-Schwinger equation (2.4) using the Schwinger-Lanczos method [41]. The equation has been solved on a grid containing typically 2000 grid points on the interval $(0, 10\ a_0)$. The Green function contained in the definition of the nonlocal potential (2.5) has been expanded into a Fourier-DVR basis set for the neutral molecule (including discretised continuum). The number of functions needed in the expansion was typically 30. Application of the Schwinger-Lanczos method for the solution of the nonlocal dynamics is described in more detail in [42, 43, 44]. We calculated $\sigma_{\mathrm{AD}}(n, J, E)$ for 300 energies up to ~ 1 eV for all the accessible final states of the molecule HX. The number of partial waves $|\psi_J\rangle$ typically needed was $J \sim 40$. We note that an extension of the calculations to energies higher than about 2 eV would require inclusion of the process of charge transfer (threshold energy between 2.5 to 3 eV for the systems of interest) and of the corresponding $\mathrm{H} + X^-$ potential.

Calculations within the LCP approximation have been performed only for $\mathrm{H} + \mathrm{Cl}^-$ and $\mathrm{H} + \mathrm{Br}^-$ collisions.

3.1. Associative detachment in H+Cl$^-$ collisions

In figure 1 we present the potential energy curves for HCl and HCl$^-$ as relevant for the present calculation. For large R both the discrete state potential $V_d(R)$ and the local complex potential $V_{\mathrm{loc}}(R)$ join the polarisation potential $-C_4R^{-4}$ (with $C_4 = 2.25$ according to the polarisability of the hydrogen atom). We start the discussion with the total AD cross sections depicted in figure 5. Our calculated cross sections (solid line), which are in good overall agreement with the experimental data of Huels *et al* [7], are decreasing with rising energy and exhibit shallow threshold structures at the opening of new final channels. These sharp structures, generally observed in halogen halides and previously discussed in [33], are a consequence of the long-range interaction of the electron with the dipole of the HX molecule (such structures are not present in the nonlocal resonance model calculation for $\mathrm{H} + \mathrm{H}^-$ [5]). For comparison we also show the cross section resulting from the local complex potential model. Although it is 10–20% smaller it is in good qualitative agreement with the nonlocal calculation. The threshold structures seen in the nonlocal calculation can not be reproduced by the local complex potential model since the potential is independent of collision energy.

The classical cross section for detachment in the long range polarisation potential is given by the Langevin cross section

$$\sigma_{\mathrm{L}} = 2\pi\sqrt{C_4/E} \tag{3.1}$$

which is also shown in figure 5. The cross section for AD is much smaller than the Langevin cross section. The reason for this behaviour is the barrier located at the internuclear distance R_B (see figure 1). To show this we constructed the following model. An infinitely sharp peak situated at R_B is added to an attractive curve (in our case the polarisation potential). If the potential at the peak is $-U_B$ then the classical cross section σ_B for the penetration through the barrier can be given in terms of the largest impact parameter $b_{\max}$ for which the effective potential $-U_B + b_{\max}^2 E/R_B^2$ is less than the collision energy E (we assume that the probability for detachment is one if the particles reach the crossing point):

$$\sigma_B = \pi b_{\max}^2 = \pi R_B^2(1 + U_B/E). \tag{3.2}$$

The overall shape of $\sigma_B(E)$ ($R_B = 3.38\ a_0$ and $U_B = 0.145$ eV for HCl) is in rather good agreement with the calculated cross sections (see figure 5) and the differences are mainly due to non-unity detachment probability and also (for larger energies) due to the idealisation of the barrier in our simple model. We thus have seen that the overall shape of the total AD cross section can be explained by a rather simple model. On the other hand the details in the spectra and the weak threshold structures in the total cross section curves are sensitive to the details of the wave function for small R where the dynamics of the system is complicated and strongly nonlocal.

To obtain a deeper understanding of the dynamics we now discuss the individual cross sections $\sigma_{v,J}(E)$. In figure 6a we plot $\sigma_{v,J}(E)$ for the collision energy 25 meV. The cross sections were normalized as follows. Instead of the cross section we plot the quantity

$$w_{v,J}(E) \equiv \frac{2\mu E}{\pi(2J+1)}\ \sigma_{v,J}(E) \tag{3.3}$$

versus impact parameter $b_J = J/\sqrt{2\mu E}$. The quantity $w_{v,J}$ is the analogue of a classical probability for detachment of the negative ion X^- coming towards H along the trajectory with impact parameter b. Although this interpretation is not absolutely correct because of the quantum-dynamical nature of the process, it gives some semiclassical insight into the dynamics. Therefore, although the exact meaning of the quantity w is given by definition (3.3) we will call it 'the detachment probability for given b'. We see that the total detachment probability is almost one for small b and quickly drops to zero at a certain impact parameter b_c. This critical value b_c is approximately equal to $b_\mathrm{c} = R_B\sqrt{1+U_B/E}$, deduced from our simple barrier model ($b_\mathrm{c} \doteq 8.8\ a_0$ for $E = 25$ meV). For each b_J most of the molecules are created in the state with the highest possible v. If b_J is increased this highest v becomes inacessible. Vanishing of the cross section for this v is compensated by an increase of the probability for all other v. This behaviour is closely related to the Wigner cusps observed in dissociative attachment cross sections [24] since AD and dissociative attachment are related by microscopic reversibility. Wigner cusps in dissociative attachment of electrons to molecules $\mathrm{H}X(v_1)$ are due to channel interaction with $v_1 \to v_2$ vibrational excitation onsets with their characteristic threshold behaviour. For associative detachment, the relevant electron energies in the process $\mathrm{H} + X^- \to \mathrm{H}X(v_1) + \mathrm{e}^-$ are those which correspond to the closing of the $\mathrm{H} + X^- \to \mathrm{H}X(v_2 > v_1) + \mathrm{e}^-$ channel. Later we will see that this energy plays also an important role in the electron spectra.

We can also see a minimum in the total detachment probability (sum of $w_{v,J}$ over v, full circles in figure 6) at the closing of one channel (here $v = 2$). We give the following interpretation of this minimum. If electrons with very small energies are detached (which is possible only near the closing of one channel) it can be turned back by the long-range dipole potential and attached again. The electron is very slow and the motion of the nuclei moving in the meantime on the potential V_0 can be reversed and after reattachment of the electron the ion X^- has a larger chance to escape. The drop in the total probability is thus the consequence of a strong coupling of electronic and nuclear motion.

All the qualitative features of the probabilities described above were already present in the calculations of Gauyacq [17] using the simplified zero-range-model for the description of the electron-HX interaction. The results of Gauyacq are shown for comparison in figure 6b; they differ from the present calculation only on the quantitative level. The behaviour of the probabilities for $b > 6$ is sensitive to the details of the potential for the HCl$^-$ ion which is seen from differences between the results obtained with Gauyacq's model A and model B (see figure 5 in [17]). Our potential lies somewhere between those of these two models as does our cut off impact parameter b_c.

The electron spectrum due to H + Cl$^-$ collisions, as calculated with the collision energy distribution in figure 4, is shown in figure 7a (solid line). Most of the electrons carry energies within the interval $\varepsilon = 0 - 0.4$ eV although the spectrum extends up to 0.95 eV. The spectrum calculated within the local complex potential model (dashed line) substantially differs from the nonlocal calculation in two regions labelled by S_1 and S_0. At these two points the nonlocal calculation predicts a sudden drop of the cross section by approximately a factor of two whereas the local calculation yields a smooth curve. Both the nonlocal and the LCP models give three further steps at energies $\varepsilon = 0.22$, 0.58 and 0.94 eV, and also some oscillations due to rotational structure are resolved. To interpret all these structures we show the partial v, J-specific cross sections $\sigma_{v,J}(R)$ in figure 7b versus the energy $\varepsilon_{v,J}$ of the released electron for the discrete collision energy $E = 110$ meV (maximum of the simulated collision energy distribution). Nonlocal results are plotted with full circles whereas open circles denote the LCP cross sections. The results presented by diamonds in figure 7b illustrate the effect of the approximation (2.18) on the cross section within the LCP model. For further explanation figure 7c presents the energies $\varepsilon_{v,J}$ as a function of orbital angular momentum J (as calculated for $E = 110$ meV). The interpretation of the steps at $\varepsilon =$ 0.22, 0.58 and 0.94 eV is straightforward. These steps correspond to the dense rotational manifold starting at $J = 0$ for $v = 2$, 1, and 0, respectively. The interpretation of the steps marked by S_1 and S_0 is more intriguing. For $v = 1$ (S_1) and $v = 0$ (S_0) there are sudden steps in the magnitude of the cross section $\sigma_{v,J}$ for $J = 13 \to J = 14$. These are due to the fact that $J = 13$ is the highest angular momentum accessible for $v = 2$. The detachment cross section is thus shared only between $v = 1$ (S_1) and $v = 0$ (S_0) for $J = 14$, whereas there is one additional accessible vibrational level ($v = 2$) for $J = 13$. Steps in the spectrum at the points S_1 and S_0 are thus explained as threshold phenomena of the same nature as Wigner cusps observed in dissociative attachment to HCl [24]. The reason that such a behaviour is not present in the spectrum calculated within the local complex potential model is due to the well known fact that the unitarity condition is not obeyed within the local complex potential model [25], i.e. the sum of $\sigma_{v,J}$ over v, J does not give exactly the total AD cross section calculated from the loss of flux in the initial channel (2.8). The cross sections $\sigma_{v,J}$ for $v = 0, 1$ thus do not "feel" the closing of the channel $v = 2$. We would like to point out another interesting feature of the structures S_1 and S_0. Unlike the other steps (due to rovibrational onsets at $J = 0$)

the structures S_1 and S_0 are sharper than the collision energy distribution itself. This is an important fact with regard to experimental observations of these structures because even for much broader collision energy distributions for which all other features of the spectra are washed out these structures will remain. The reason for this behaviour is the fact that the position of the steps is insensitive to collision energy. The energy position $\varepsilon(S_{v_1,v_2})$ of the structure S_{v_1,v_2} occuring for the vibratonal level v_1 due to rotational channel closing at J_m for a vibrational level $v_2 > v_1$ is given by

$$\begin{aligned}\varepsilon(S_{v_1,v2}) &= G_{v_2} - G_{v_1} + F_{v_2}(J_m) - F_{v_1}(J_m) \\ &\approx G_{v_2} - G_{v_1} + (B_{v_2} - B_{v_1})J_m(J_m+1),\end{aligned} \tag{3.4}$$

where G_v and $F_v(J)$ denote the vibrational and rotational energies and B_v the rotatonal constants. Although J_m depends on collision energy $E_{\rm rel}$, the energy $\varepsilon(S_{v_1,v_2})$ is (almost) independent of $E_{\rm rel}$ since the difference of the rotational energies in (3.4) varies negligibly with $J_m(E_{\rm rel})$ for reasonably small variation of $E_{\rm rel}$. To first order $\varepsilon(S_{v_1,v_2})$ is simply given by $G_{v_2} - G_{v_1}$.

The information contained in the electron spectrum is in some sense equivalent to knowledge of the state distribution of the product molecule HCl. This distribution has been determined experimentally by analyzing the infrared light emission from the molecules HCl formed by associative detachment at a temperature of $T = 296$ K [10]. To compare with this type of experiment which yields rotationally summed and collision-energy averaged rate coefficients k_v we averaged the cross sections $\sigma_{v,J}$ over the appropiate thermal Maxwell-Boltzmann collision energy distribution times the relative collisional velocity

$$F(E_{\rm rel}) = (k_B T)^{-2}\ E_{\rm rel}\ \exp(-E_{\rm rel}/k_B T), \tag{3.5}$$

at the relevant temperature ($T = 296$ K) and therebye obtained product state distributions $p_{v,J}$, i.e. probabilities for AD into final states (v, J). The quantity $p_{v,J}$ is defined by

$$p_{v,J} = \frac{1}{N} \int \sigma_{v,J}(E_{\rm rel})\ F(E_{\rm rel})\ {\rm d}E_{\rm rel}. \tag{3.6}$$

Here N is a normalization constant such that $\sum p_{v,J} = 1$ when the sum is extended over all accesible states (v, J). The product state distributions for HCl(v, J) are given in table 1. The same table shows also the sum p_v of the probabilities $p_{v,J}$ over all J, i.e. the rotationally summed vibrational distribution. The same quantity is shown also for the LCP approximation and for the zero range potential model† of Gauyacq [17]. The population of the states is not measured directly in the experiment of Zwier et. al. [10] who give the ratio $p_2/p_1 = 0.60 \pm 0.03$. In our nonlocal resonance model calculation we obtain $p_2/p_1 = 0.57$, and Model B of Gauyacq yields 0.61 (note that the experimental value for p_2/p_1 was actually used for the construction of the theoretical model in [17]). Both values are close to the experiment, while the LCP model gives the value 1.32.

† The results shown in the table are obtained with model B. Model A gives $p_2/p_1 = 0.25$ (see [17]).

3.2. Associative detachment in H+F$^-$, H+Br$^-$ and D+F$^-$ collisions

In figures 8 and 9 we present the energy dependent total AD cross sections for $\mathrm{H} + \mathrm{F}^-$ and $\mathrm{H}+\mathrm{Br}^-$ collisions. Unlike the case of $\mathrm{H}+\mathrm{Cl}^-$, no barrier is present in the potential for $\mathrm{H} + \mathrm{F}^-$, and the calculated total AD cross sections for $\mathrm{H} + \mathrm{F}^-$ are close to the corresponding Langevin cross sections (3.1), i.e. all close collisions have detachment probabilities close to unity. At low collision energies the small difference between σ_{AD} and σ_{L} is mainly due to the small difference of the detachment probabilities at small internuclear distances from unity; for higher energies the deviation of the full potential from the polarization potential becomes important. Similar to the $\mathrm{H} + \mathrm{Cl}^-$ case, a substantial barrier is present for $\mathrm{H} + \mathrm{Br}^-$ ($R_{\mathrm{B}} = 3.38$ a_0, $U_{\mathrm{B}} = 0.116$ eV, see also [39]) and the calculated cross sections σ_{AD} (solid line in figure 9) are found to be substantially lower than the Langevin cross section σ_{L} (dot-dashed line) for kinetic energies below 1 eV. As for the case $\mathrm{H} + \mathrm{Cl}^-$, the AD cross sections obtained for $\mathrm{H} + \mathrm{Br}^-$ with our simple barrier model (dotted line in figure 9) follow closely the cross sections obtained with the full calculation.

Electron spectra for $\mathrm{H} + \mathrm{F}^-$ and $\mathrm{H} + \mathrm{Br}^-$, calculated with the collision energy distributions shown in figure 4, are presented in figures 10 and 11. In the comparison of the electron spectra shown in figures 7, 10, 11 it is important to keep in mind the different mean values and widths in the collision energies for the three systems. With rising kinetic energies the number of contributing orbital angular momenta J increases. The broader the width of the collision energy distribution, the lower the effective energy resolution in the electron spectrum. Correspondingly, the $\mathrm{H} + \mathrm{F}^-$ is characterised by the largest J range and the broadest energy width. Nevertheless, rotational structure in the $\mathrm{H} + \mathrm{F}^-$ spectrum is still resolved due to the fact that the rotational constant is largest for HF and that the rotational spacings increase, of course, with rising J (see figure 10). For spectrometer bandwidths below about 10 meV, the rotational structure in the $\mathrm{H} + \mathrm{Br}^-$ spectrum could be resolved to a large extent (see figure 11) since the collision energy distribution for this system is sufficiently narrow. With a spectrometer width of 30 meV, details of the rotational structure are essentially washed out (thick line in figure 11).

At low collision energies, the number of accessible vibrational states is 6 for HF, 3 for HCl, and 2 for HBr. Correspondingly, the spectrum extends up to 2.6 eV for HF, to 0.95 eV for HCl, and to 0.45 eV for HBr, but most of the electrons carry energies within the range 0 to 0.5 eV: note that penetration of the $\mathrm{H}+X^-$ system towards very low distances (where the largest electron energies are emitted) is only possible for low angular momenta J (for which the cross section is small) and , in addition, survival of the $\mathrm{H}+X^-$ system down to small distances is small. The Wigner-type cusps, discussed in detail for $\mathrm{H}+\mathrm{Cl}^-$, cause steps also in the spectra for $\mathrm{H}+\mathrm{F}^-$ and $\mathrm{H}+\mathrm{Br}^-$ (see figures 10 and 11). These steps are not present in the LCP results for HBr in figure 11. For HF, these steps happen to coincide with steps due to the rovibrational onsets for $J = 0$, but this coincidence would disappear for different (mean) collision energies, since the steps associated with the rotational onsets shift with collision energy. This effect is seen in figure 12 showing the calculated electron spectrum for the collision energy 50 meV. The same figure allows for a direct comparison with the spectrum for HBr for the same collision energy in figure 11b).

In Tables 2 and 3 we list the rovibrational product state distributions calculated for AD in $H + F^-$ and $H + Br^-$ collisions at thermal kinetic energies (Maxwellian kinetic energy distribution at $T \approx 300$ K). For each vibrational level the rotational populations p_{vJ} at low J are found to rise according to the statistical weights $(2J + 1)$ (this is true for the p_{vJ} in all systems studied here) while towards higher J the behaviour reflects also the varying Franck-Condon factors and the nonlocal dynamics. For $H+Br^-$, no previous theoretical or experimental results for rotationally specific or rotationally-summed populations p_v are available to our knowledge. At $T = 300$ K, HBr(v) is almost only formed in the vibrational levels $v = 0$ and 1; our calculations predict a population ratio of p_1/p_0= 0.70 (this is inverted for the LCP calculation: p_1/p_0= 1.35). For the systems $H + F^-$ and $D + F^-$ our populations p_v can be compared with the zero-range calculations of Gauyacq [17] (for HF) and with the experimental data, derived from infrared emission spectroscopy in a flow system [12]. For HF(v) formation, there is good overall agreement between the three results with the highest population being consistently found for $v = 4$. With the exception of $v = 1$ (for which the experimental value is somewhat high) the agreement between experiment and the nonlocal theory is excellent. The situation is less satisfactory for the system $D + F^-$: compared to the theoretical results the experimental distribution p_v is broader and shifted towards lower vibrational levels with a lower amount of energy deposited into vibration than for HF. Smith and Leone discussed this problem in some detail in comparison with the theoretical results of Gauyacq [17] (which exhibit the same trend as our results) and concluded that “there is presently no reasonable explanation for the large difference in vibrational populations between HF and DF”. As cited in [12] by Smith and Leone, Gauyacq also found - in qualitative agreement with our results - that the fraction of energy deposited into vibration is identical for HF and DF at thermal collision energies. Based on recent reconsiderations of vibrational relaxation processes and of possible problems in the uniqueness of the data analysis (which might be more severe for DF than for HF) Smith and Leone concluded [46] that there is no obvious cause which could have affected the DF results in the observed direction, namely a shift towards lower vibrational energies.

4. Conclusions and perspectives

In this paper we have presented total and final-state specific absolute cross sections for low-energy associative detachment (AD) in the collision systems $H + F^-$, $D + F^-$, $H + Cl^-$, and $H + Br^-$, as obtained with a nonlocal resonance theory involving realistic potentials. The total, energy-dependent AD cross sections are in good agreement with the experimental data of Huels *et al* [6]. For the systems $H + F^-$ and $D + F^-$ the total

AD cross section is close to the Langevin capture cross section. For $H+Cl^-$ and $H+Br^-$, on the other hand, the total AD cross sections are strongly influenced by a repulsive barrier in the (real part of the) negative ion potential, and the AD cross sections are substantially smaller than the Langevin cross sections at kinetic energies below 1 eV.

Final state specific cross sections $\sigma_{vJ}(E)$ for fixed collision energy E prefer the highest accessible v for each J. Steps in the J dependence of the partial cross sections σ_{vJ} are observed at a particular J' when a vibrational level with $v' > v$ becomes energetically forbidden for $J > J'$. These steps are directly related by microscopic reversibility to Wigner cusps observed in the reverse process of AD, namely dissociative electron attachment $\mathrm{H}X + \mathrm{e}^- \to \mathrm{H} + X^-$. We emphasize that these steps cannot be predicted when one uses a local complex potential model to describe the AD process. In the electron energy spectra for AD in a particular system, the steps occur at essentially fixed electron energies and almost independent of collision energy, and can therefore be observed with rather broad collision energy distributions and with rather modest electron energy resolution. To our knowledge, these steps have not been reported experimentally so far.

Electron energy spectra have been calculated for collision energy distributions which correspond to realistic conditions for a low energy crossed beams experiment involving a $T = 300$ K hydrogen atom beam and a negative halogen ion beam with a kinetic energy of 5 eV. The maximum cross sections $\mathrm{d}\sigma/\mathrm{d}\varepsilon$ in these calculated electron spectra are the same within a factor of two, and an estimate shows that such an experiment may in fact be feasible. With negative ion beams of 10^{10}/s (about 2 nA), hydrogen atom densities of $10^{12}/\mathrm{cm}^3$, overall angle- differential electron spectrometer detection efficiencies of 10^{-4} at 20 meV resolution bandwidth, target path lengths of 0.3 cm one expects maximum electron counting rates of (30–60)/s.

The nascent rovibrational state distributions for the $\mathrm{H}X(v, J)$ molecules formed in the AD process with a thermal kinetic energy distribution at a temperature of $T = 300$ K have also been calculated. For HF and HCl, the results of the calculations of Gauyacq [17] which involve the zero-range potential approximation for the $\mathrm{H}X + \mathrm{e}^-$ interaction and include non-adiabatic nuclear motion effects, are in good qualitative agreement with the present calculations using the nonlocal resonance theory (including the step structure in the electron spectra). The experimental results for the vibrational populations p_v in HF(v) and HCl(v), derived from infrared emission spectra by Smith and Leone [12], are in good overall agreement with the theoretical results while their data for DF(v) yield substantially less vibrational excitation than the calculations. In view of the fact that the nonlocal resonance theory, used here for the description of associative detachment, has been very successful in describing details of vibrational excitation and dissociative attachment in electron-HX collisions for HF [45], HCl [33] and HBr [39] at low energies, we have difficulties to attribute the difference between the experimental values for the vibrational population in DF(v) and our calculated results to deficiencies in the theory applied in the present work.

Acknowledgments

This work has been supported by the Deutsche Forschungsgemeinschaft (Forschergruppe Niederenergetische Elektronenstreuprozesse). We gratefully acknowledge S.R. Leone, M. Smith, J.P. Gauyacq, F. Linder and M.-W. Ruf for useful discussion and I.I. Fabrikant and Y. Xu for providing their data for construction of the model for HF. M. Čížek acknowledges members of the Forschergruppe for their hospitality during stays in Kaiserslautern and Heidelberg.

References

[1] Massey H S W 1976 *Negative ions* (Cambridge: Cambridge University Press)
[2] Esaulov V A 1986 *Ann. Phys. Fr.* **11** 493
[3] Bieniek R J and Dalgarno A 1979 *Astrophys. J.* **228** 635
[4] Launay J M, Le Dourneuf M and Zeippen C J 1991 *Astron. Astrophys.* **252** 842
[5] Čížek M, Horáček J and Domcke W 1998 *J. Phys. B* **31** 2571
[6] Huels M A, Champion R L, Doverspike L D and Wang Y 1990 *Phys. Rev. A* **41** 4809
[7] Huels M A, Fedchak J A, Champion R L, Doverspike L D, Gauyacq J P and Teillet-Billy D 1994 *Phys. Rev. A* **49** 255
[8] Fedchak J A, Huels M A, Doverspike L D and Champion R L 1993 *Phys. Rev. A* **47** 3796
[9] Fedchak J A, Champion R L, Doverspike L D and Wang Y 1994 *J. Phys. B* **27** 3045
[10] Zwier T S, Maricq M M, Simpson C J S M, Bierbaum V M, Ellison G B and Leone S R 1980 *Phys. Rev. Lett.* **44** 1050
[11] Zwier T S, Weisshaar J C and Leone S R 1981 *J. Chem. Phys.* **75** 4885
[12] Smith M A and Leone S R *J. Chem. Phys.* **78** 1325
[13] Howard C J, Fehsenfeld F C and McFarland M *J. Chem. Phys.* **60** 5086
[14] Fehsenfeld F C 1975 *Interactions between ions and molecules* edited by Pierre J. Ausloos (New York: Plenum)
[15] Smith D and Adams N G 1987*J. Phys. B* **20** 4903
[16] Huq M S, Fraedrich D S, Doverspike L D, Champion R L and Esaulov V A 1982 *J. Chem. Phys.* **76** 4952
[17] Gauyacq J P 1982 *J. Phys. B* **15** 2721
[18] Bieniek R J 1978 *Phys. Rev. A* **18** 392
[19] Domcke W 1991 *Phys. Rep.* **208** 97
[20] Mizuno J and Chen J C Y 1969 *Phys. Rev.* **187** 167
[21] Sakimoto K 1989 *Chem. Phys. Lett.* **164** 294
[22] Müller M W, Merz A, Ruf M, Hotop H, Meyer W and Movre M 1991 *Z. Phys. D* **21** 89
[23] Bardsley N and Wadehra J M 1983 *J. Chem. Phys* **78** 7227
[24] Abouaf R and Teillet-Billy D 1977 *J. Phys. B* **10** 2261
[25] Bieniek R J 1980 *J. Phys. B* **13** 4405
[26] Domcke W and Cederbaum L S 1980 *J. Phys. B* **14** 149
[27] Domcke W and Mündel C 1985 *J. Phys. B* **18** 4491
[28] Gertitschke P L and Domcke W 1994 *Z. Phys. D* **31** 171
[29] Horáček J and Domcke W 1996 *Phys. Rev. A* **53** 2262
[30] Horáček J, Domcke W and Nakamura H 1997 *Z. Phys. D* **42** 181
[31] Mündel C, Berman M and Domcke W 1985 *Phys. Rev. A* **32** 181
[32] Gallup G A, Xu Y and Fabrikant I I 1998 *Phys. Rev. A* **57** 2596
[33] Čížek M , Horáček J and Domcke W 1999 *Phys. Rev. A* **60** 2873
[34] Gauyacq J P 1985 *J. Phys. B* **18** 1859
[35] Teillet-Billy D and Gauyacq J P 1984 *J. Phys. B* **17** 4041

[36] Estrada H, Cederbaum L S and W Domcke 1986 *J. Chem. Phys.* **86** 152
[37] Berman M, Mündel C and Domcke W 1985 *Phys. Rev. A* **31** 641
[38] Movre M and Meyer W 1997 *J. Chem. Phys.* **106** 7139
[39] Čížek M, Horáček J, Sergenton A-Ch, Popović D B, Allan M, Leininger T and Gadea F X (in preparation)
[40] Piecuch P 1997 *J. Mol. Structure* **436–437** 503
[41] Meyer H-D, Horáček J and Cederbaum L S 1991 *Phys. Rev. A* **43** 3587
[42] Horáček J 1995 *J. Phys. B* **28** 1585
[43] Horáček J, Gemperle F and Meyer H-D 1996 *J. Chem. Phys.* **104** 8433
[44] Horáček J, Čížek M and Domcke W 1998 *Theor. Chem. Acc.* **100** 31
[45] Xu Y, Gallup G A and Fabrikant I I 1999 *Phys. Rev. A* **61** 052705–1
[46] Smith M and Leone S R, private communication (2000)

Table 1. Product state distribution $p_{v,J}$ for the reaction $\mathrm{H} + \mathrm{Cl}^- \rightarrow \mathrm{HCl}(v, J) + \mathrm{e}^-$, calculated for a Maxwellian collision energy distribution (3.5) at T = 296 K.

J	v=0	v=1	v=2
0	0.124E-3	0.113E-2	0.318E-2
1	0.373E-3	0.339E-2	0.954E-2
2	0.628E-3	0.570E-2	0.158E-1
3	0.893E-3	0.808E-2	0.220E-1
4	0.117E-2	0.106E-1	0.281E-1
5	0.147E-2	0.132E-1	0.338E-1
6	0.179E-2	0.160E-1	0.389E-1
7	0.215E-2	0.190E-1	0.432E-1
8	0.257E-2	0.224E-1	0.462E-1
9	0.293E-2	0.252E-1	0.444E-1
10	0.409E-2	0.343E-1	0.312E-1
11	0.656E-2	0.535E-1	0.126E-1
12	0.909E-2	0.720E-1	0.457E-2
13	0.109E-1	0.835E-1	0.148E-2
14	0.105E-1	0.773E-1	0.422E-3
15	0.870E-2	0.611E-1	0.911E-4
16	0.566E-2	0.376E-1	0.239E-5
17	0.332E-2	0.205E-1	
18	0.214E-2	0.118E-1	
19	0.120E-2	0.564E-2	
20	0.170E-2	0.241E-2	
21	0.906E-3	0.587E-3	
22	0.320E-3	0.105E-3	
23	0.973E-4	0.248E-5	
24	0.146E-4		
25	0.384E-5		
26	0.102E-5		
Sum	0.079	0.585	0.336
LCP	0.038	0.415	0.547
Gauyacq	0.099	0.559	0.342

Table 2. Product state distribution $p_{v,J}$ for the reaction $\mathrm{H} + \mathrm{F}^- \rightarrow \mathrm{HF}(v, J) + \mathrm{e}^-$, calculated for a Maxwellian collision energy distribution (3.5) at T = 298 K.

J	v=0	v=1	v=2	v=3	v=4	v=5	v=6
0	0.796E-7	0.242E-5	0.332E-4	0.163E-3	0.663E-3	0.275E-2	0.444E-5
1	0.242E-6	0.736E-5	0.100E-3	0.491E-3	0.201E-2	0.825E-2	0.114E-4
2	0.413E-6	0.126E-4	0.170E-3	0.826E-3	0.341E-2	0.138E-1	0.138E-4
3	0.596E-6	0.183E-4	0.243E-3	0.117E-2	0.489E-2	0.192E-1	0.120E-4
4	0.799E-6	0.247E-4	0.320E-3	0.152E-2	0.645E-2	0.244E-1	0.816E-5
5	0.101E-5	0.313E-4	0.395E-3	0.184E-2	0.799E-2	0.288E-1	0.431E-5
6	0.129E-5	0.402E-4	0.491E-3	0.225E-2	0.993E-2	0.335E-1	0.185E-5
7	0.164E-5	0.515E-4	0.605E-3	0.271E-2	0.122E-1	0.380E-1	0.542E-6
8	0.200E-5	0.634E-4	0.714E-3	0.312E-2	0.144E-1	0.401E-1	0.699E-8
9	0.257E-5	0.818E-4	0.876E-3	0.370E-2	0.175E-1	0.416E-1	
10	0.327E-5	0.106E-3	0.106E-2	0.429E-2	0.213E-1	0.368E-1	
11	0.672E-5	0.216E-3	0.184E-2	0.760E-2	0.428E-1	0.729E-2	
12	0.900E-5	0.267E-3	0.211E-2	0.958E-2	0.505E-1	0.113E-2	
13	0.117E-4	0.320E-3	0.239E-2	0.117E-1	0.557E-1	0.153E-3	
14	0.132E-4	0.338E-3	0.240E-2	0.123E-1	0.524E-1	0.172E-4	
15	0.157E-4	0.372E-3	0.251E-2	0.134E-1	0.492E-1	0.125E-5	
16	0.179E-4	0.393E-3	0.251E-2	0.138E-1	0.413E-1		
17	0.220E-4	0.442E-3	0.263E-2	0.152E-1	0.297E-1		
18	0.459E-4	0.756E-3	0.462E-2	0.296E-1	0.198E-2		
19	0.464E-4	0.698E-3	0.468E-2	0.266E-1	0.102E-3		
20	0.479E-4	0.668E-3	0.471E-2	0.229E-1	0.390E-5		
21	0.400E-4	0.521E-3	0.377E-2	0.149E-1			
22	0.445E-4	0.532E-3	0.395E-2	0.107E-1			
23	0.672E-4	0.775E-3	0.644E-2	0.586E-3			
24	0.674E-4	0.841E-3	0.607E-2	0.127E-4			
25	0.397E-4	0.509E-3	0.307E-2				
26	0.146E-4	0.188E-3	0.887E-3				
27	0.113E-4	0.154E-3	0.256E-3				
28	0.475E-5	0.651E-4	0.295E-5				
29	0.116E-5	0.136E-4					
30	0.312E-6	0.294E-5					
31	0.549E-8	0.336E-7					
32	0.250E-8						
Sum	0.541E-3	0.851E-2	0.060	0.211	0.424	0.296	0.565E-4
Gauyacq			0.05	0.23	0.48	0.23	
Exp.		$0.0^{+0.06}_{-0.0}$	0.09 ± 0.01	0.21 ± 0.01	0.41 ± 0.02	0.30 ± 0.02	

Table 3. Product state distribution $p_{v,J}$ for the reaction $\mathrm{H} + \mathrm{Br}^- \rightarrow \mathrm{HBr}(v, J) + \mathrm{e}^-$, calculated for a Maxwellian collision energy distribution (3.5) at T = 300 K.

J	v=0	v=1	v=3
0	0.989E-3	0.430E-2	0.418E-6
1	0.299E-2	0.129E-1	0.111E-5
2	0.504E-2	0.214E-1	0.166E-5
3	0.719E-2	0.298E-1	0.177E-5
4	0.950E-2	0.379E-1	0.175E-5
5	0.121E-1	0.458E-1	0.146E-5
6	0.151E-1	0.530E-1	0.110E-5
7	0.190E-1	0.592E-1	0.749E-6
8	0.249E-1	0.628E-1	0.466E-6
9	0.503E-1	0.439E-1	0.255E-6
10	0.824E-1	0.224E-1	0.131E-6
11	0.943E-1	0.108E-1	0.643E-7
12	0.851E-1	0.460E-2	0.293E-7
13	0.633E-1	0.185E-2	0.120E-7
14	0.572E-1	0.649E-3	0.439E-8
15	0.278E-1	0.218E-3	0.158E-8
16	0.154E-1	0.703E-4	
17	0.830E-2	0.197E-4	
18	0.420E-2	0.531E-5	
19	0.201E-2	0.138E-5	
20	0.894E-3	0.312E-6	
21	0.344E-3	0.680E-7	
22	0.117E-3	0.138E-7	
23	0.359E-4	0.259E-8	
24	0.997E-5		
25	0.240E-5		
26	0.522E-6		
27	0.937E-7		
28	0.152E-7		
29	0.229E-8		
Sum	0.588	0.412	0.110E-4
LCP	0.426	0.574	0.845E-5

Table 4. Rotationally-summed product state distribution p_v for the reaction D+F$^-$ $\rightarrow$ DF(v, J) + e$^-$, calculated for a Maxwellian collision energy distribution (3.5) at $T = 298$ K. (Rotational distributions can be obtained from the authors upon request.)

	v=0	v=1	v=2	v=3	v=4
Theory	1.80E-5	4.19E-4	4.09E-3	0.025	0.084
Exp.		$0.08^{+0.01}_{-0.07}$	0.09 ± 0.01	0.15 ± 0.02	0.11 ± 0.02

	v=5	v=6	v=7	v=8	v=9
Theory	0.197	0.313	0.320	0.057	0.151E-5
Exp.	0.15 ± 0.01	0.24 ± 0.03	0.18 ± 0.02	-	-

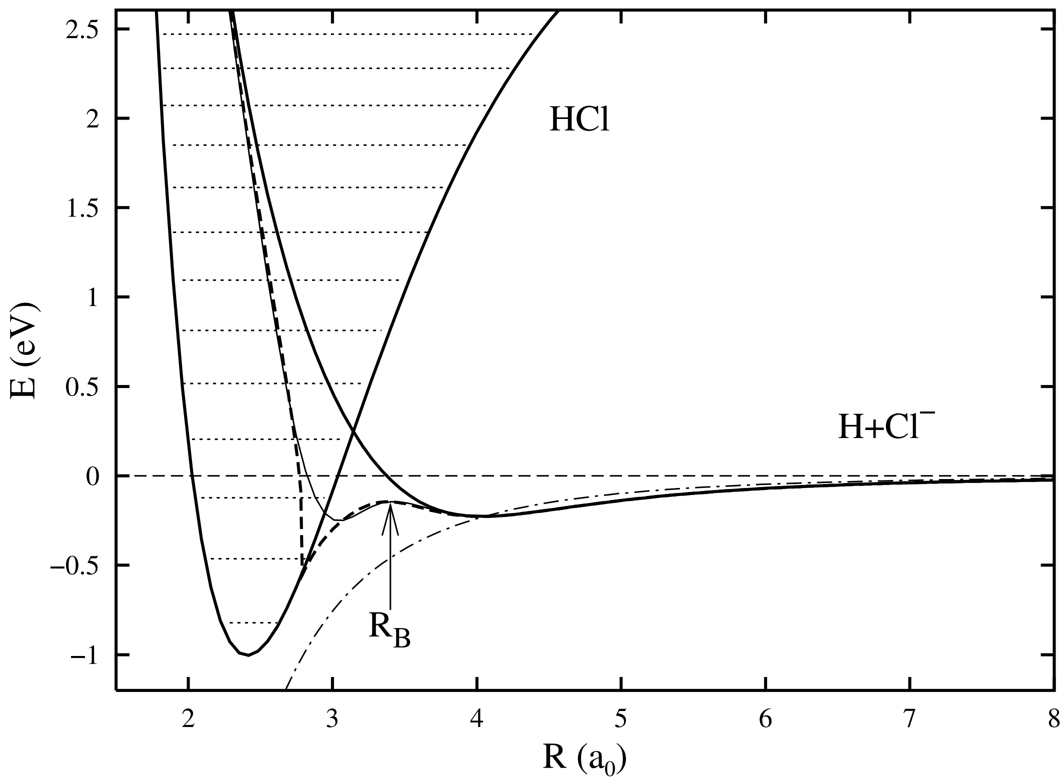

Figure 1. Potential energy curves for HCl and HCl$^-$. The thick solid lines show the potentials $V_0(R)$ and $V_d(R)$ and the dashed line the energy of the HCl$^-$ bound state which becomes a resonance for small R. Bound states in $V_0(R)$ are indicated with dots and the H + Cl$^-$ asymptote with dashes. Dotted-dashed line shows the polarisation potential $-2.25R^{-4}$. The thin solid line denotes the real part of the local complex potential (see text).

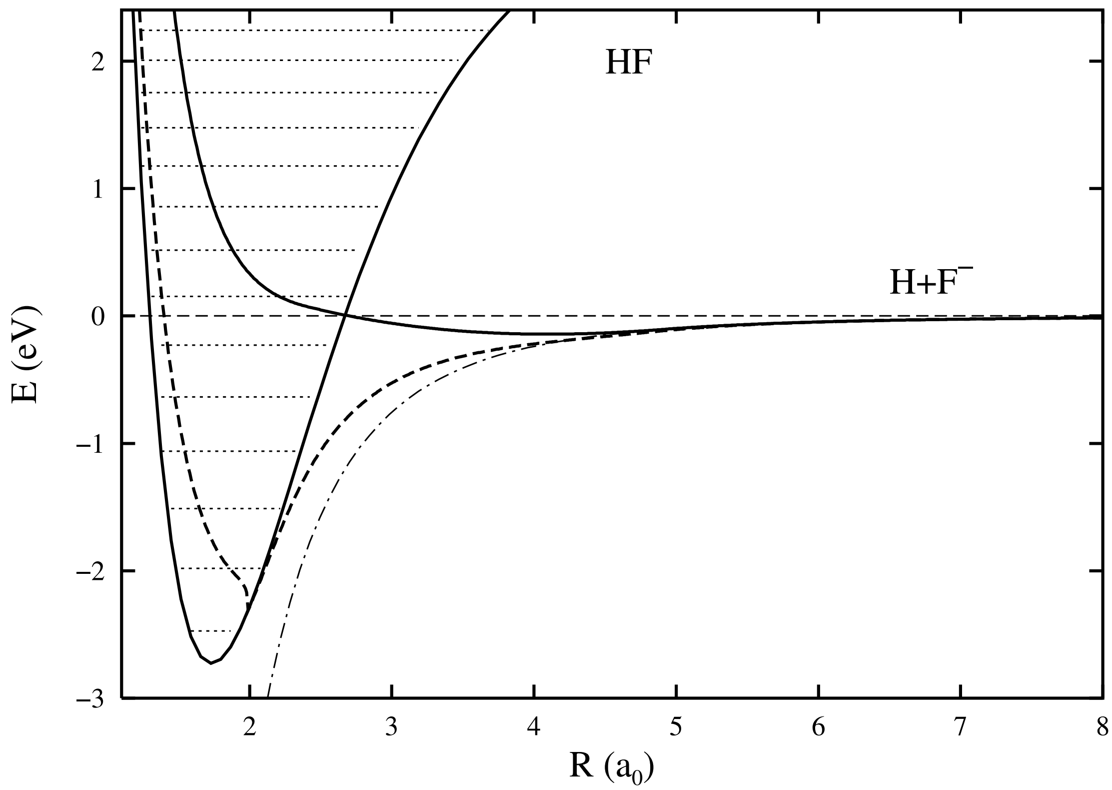

Figure 2. Potential energy curves for HF and HF$^-$. Meaning of the symbols is the same as in figure 1.

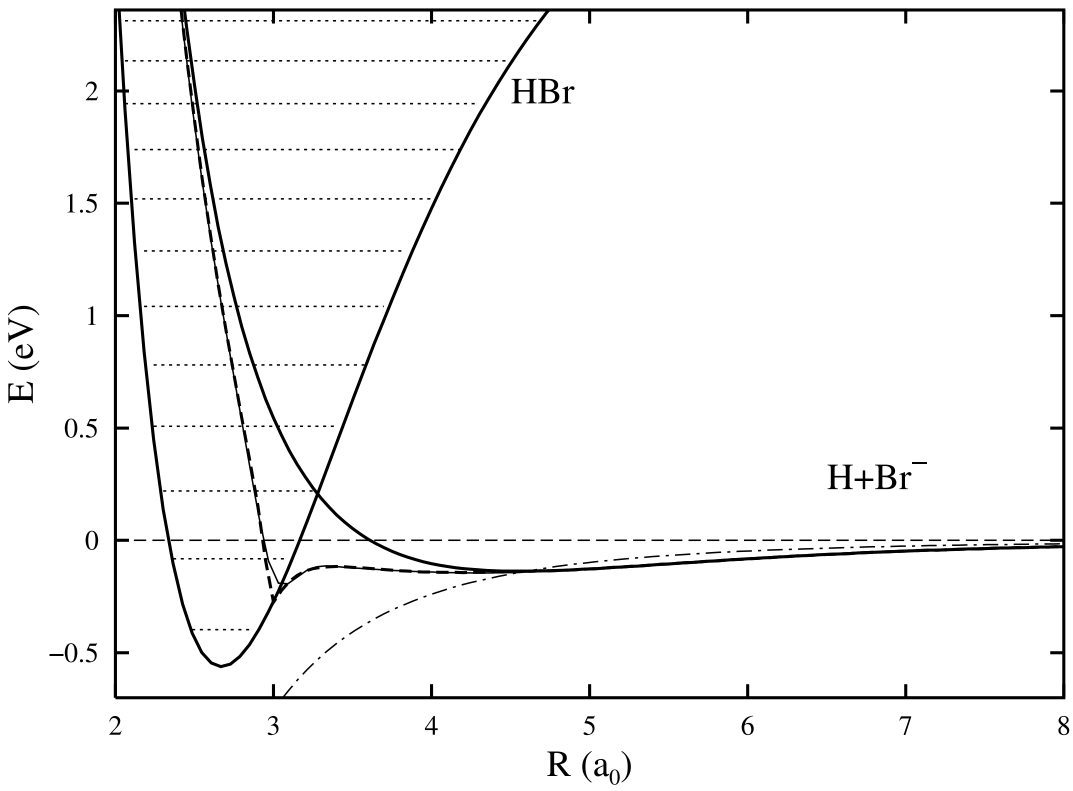

Figure 3. Potential energy curves for HBr and HBr$^-$. Meaning of the symbols is the same as in figure 1.

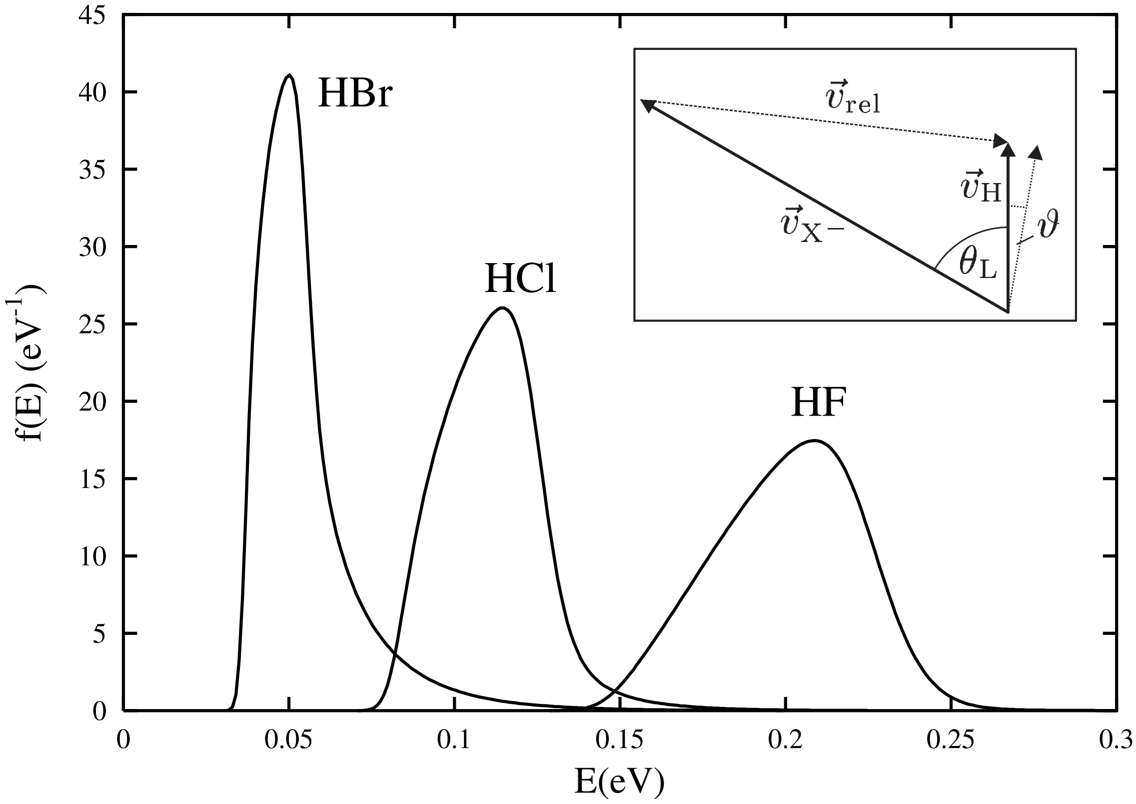

Figure 4. Collision energy distributions for $\mathrm{H} + X^-$ ($X = \mathrm{Br}, \mathrm{Cl}, \mathrm{F}$), as relevant for simulating electron energy spectra for associative detachment in beam experiments. The negative halogen ion-beam is assumed to have a Gaussian energy distribution with an average kinetic energy of $E_0 = 5$ eV and an energy width of 0.5 eV (FWHM). The thermal hydrogen beam is described by a Maxwell-Boltzmann distribution with $T = 300$ K. In the calculations, a laboratory collision angle of $\theta_{\rm L} = 60°$ is used. ϑ denotes the maximum deviation of the direction of the hydrogen beam from its nominal direction (see text for more information).

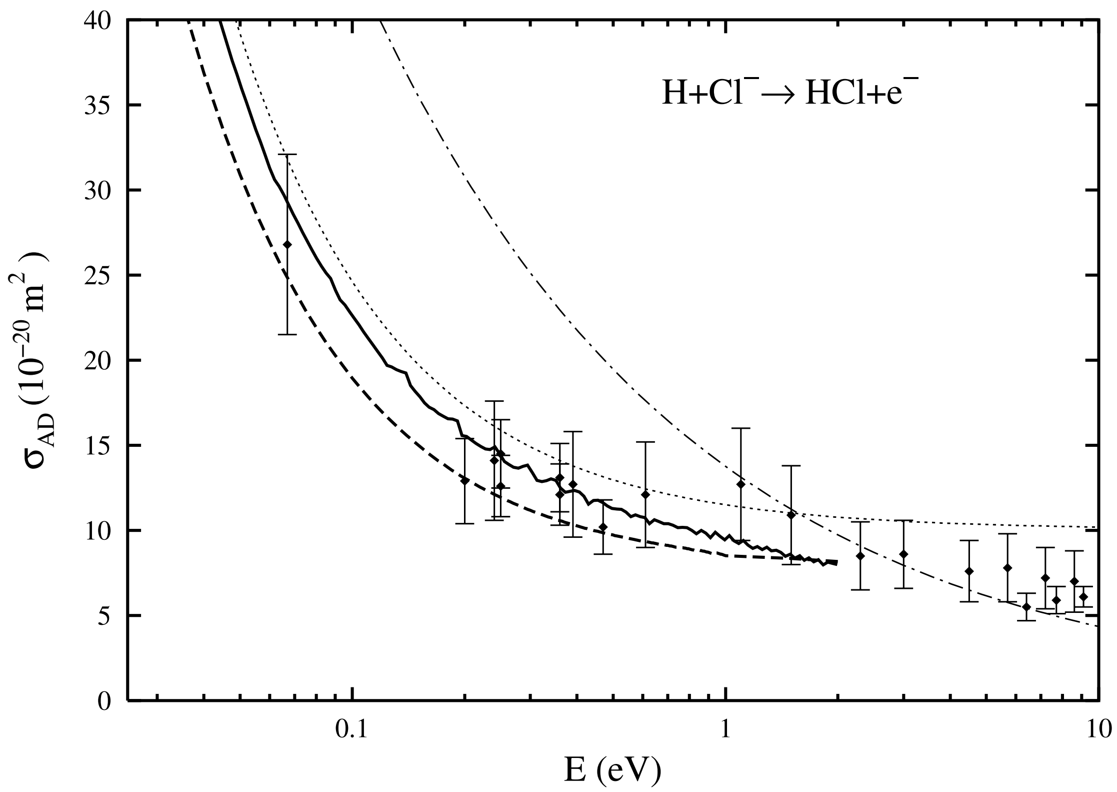

Figure 5. The calculated total AD cross section (solid line) and the experimental data of Huels *et al* [7] (diamonds with errorbars). The dotted-dashed line shows the Langevin cross section and the dotted line the cross section for the simple barrier model described in the text. The dashed line represents the results of the calculations employing the local complex potential.

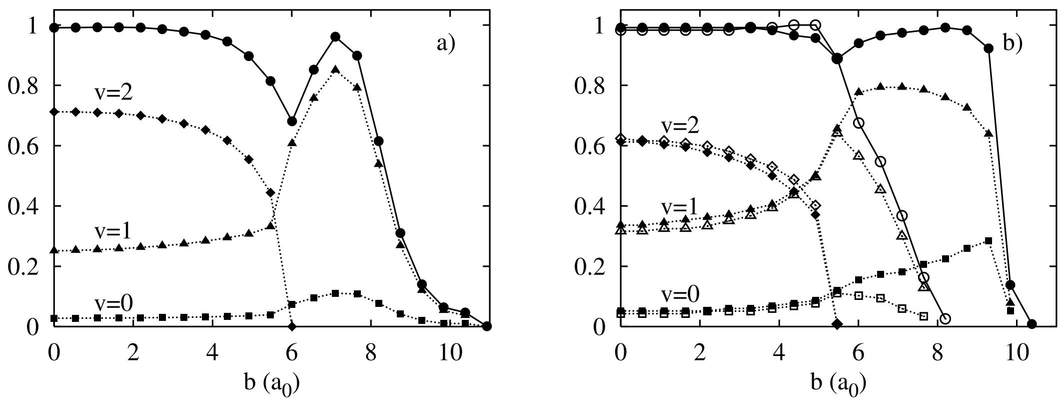

Figure 6. a) Dependence of the detachment probability in $Cl^- + H$ collisions on the impact parameter for the discrete collision energy 25 meV (•). Contributions from the different final vibrational states are shown by squares ($v = 0$), triangles ($v = 1$), and diamonds ($v = 2$) and for better recognition connected by dotted lines.
b) The same as a) according to the calculation of Gauyacq [17]. Results reported for model A and B in [17] are denoted by full and open symbols, respectively.

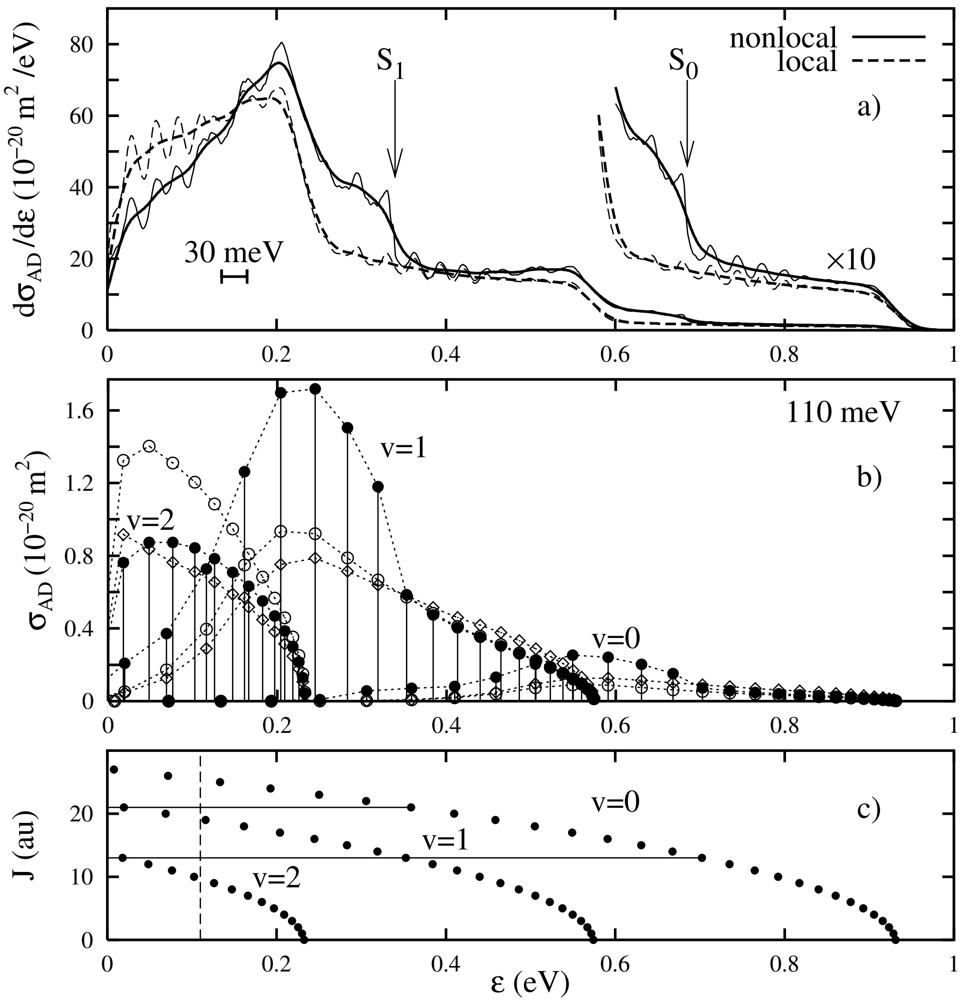

Figure 7. Results for associative detachment in H + Cl$^-$ collisions. **a)** Energy spectrum of electrons released in H + Cl$^-$ collisions for the collision energy distribution shown in figure 4 (average collision energy: 110 meV) **b)** Cross sections $\sigma_{vJ}(E)$, calculated at the discrete collison energy E_{rel} = 110 meV versus electron energy $\varepsilon_{v,J}$. Full circles: results of nonlocal theory; open cirles: LCP results; open diamonds: LCP results with additional assumption (2.18). **c)** Dependence of the electron energy $\varepsilon_{v,J}$ on orbital angular momentum J (at E_{rel} = 110 meV), illustrating the ranges of J with a different number of accessible final vibrational states.

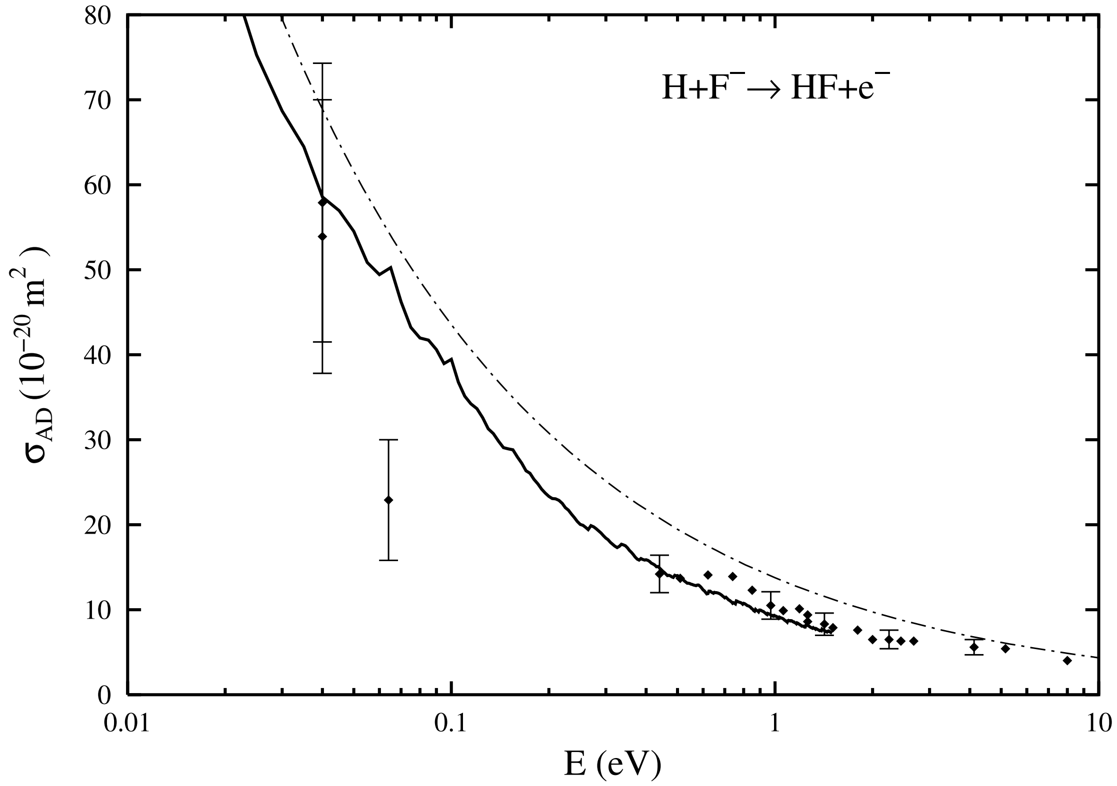

Figure 8. Total associative detachment cross section for H + F$^-$. The meaning of the symbols is the same as in figure 5.

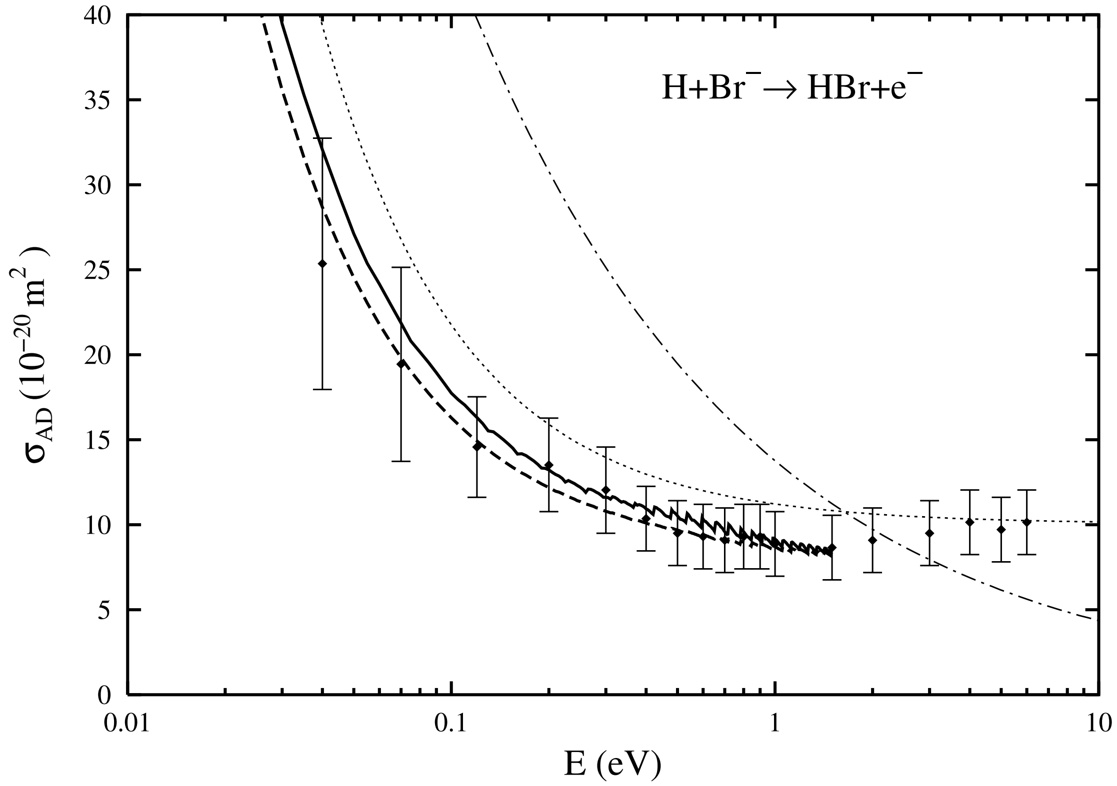

Figure 9. Total associative detachment cross section for $H + Br^-$. The meaning of the symbols is the same as in figure 5.

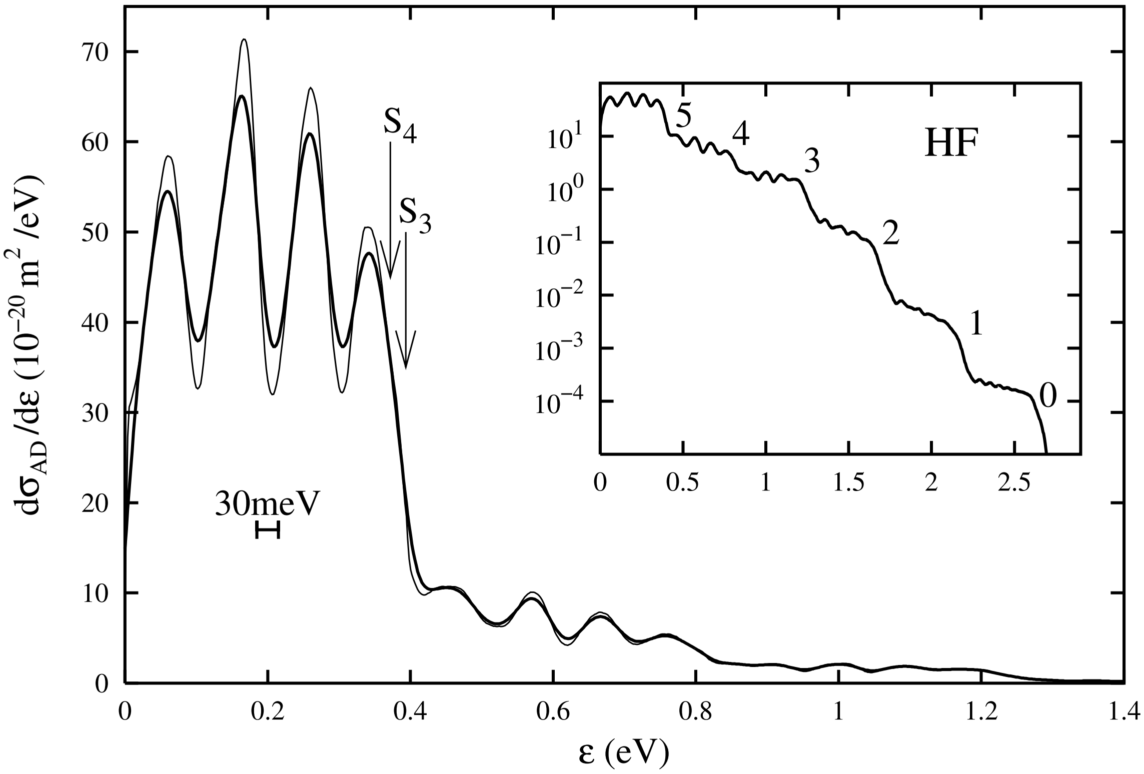

Figure 10. Electron spectrum for associative detachment in H + F^- collisions for the the collision energy distribution shown in figure 4. The spectrum shown with thick line is convoluted with a typical electron spectrometer resolution of 30 meV (FWHM). S_3 and S_4 denote the step-like increase of the rovibrational population in the nonlocal calculation for $v = 3$ and $v = 4$ associated with the closing of the $v = 4$ and $v = 5$ channel, respectively. In the insert the whole spectrum (extending over 6 orders of magnitude) is shown on a logarithmic scale.

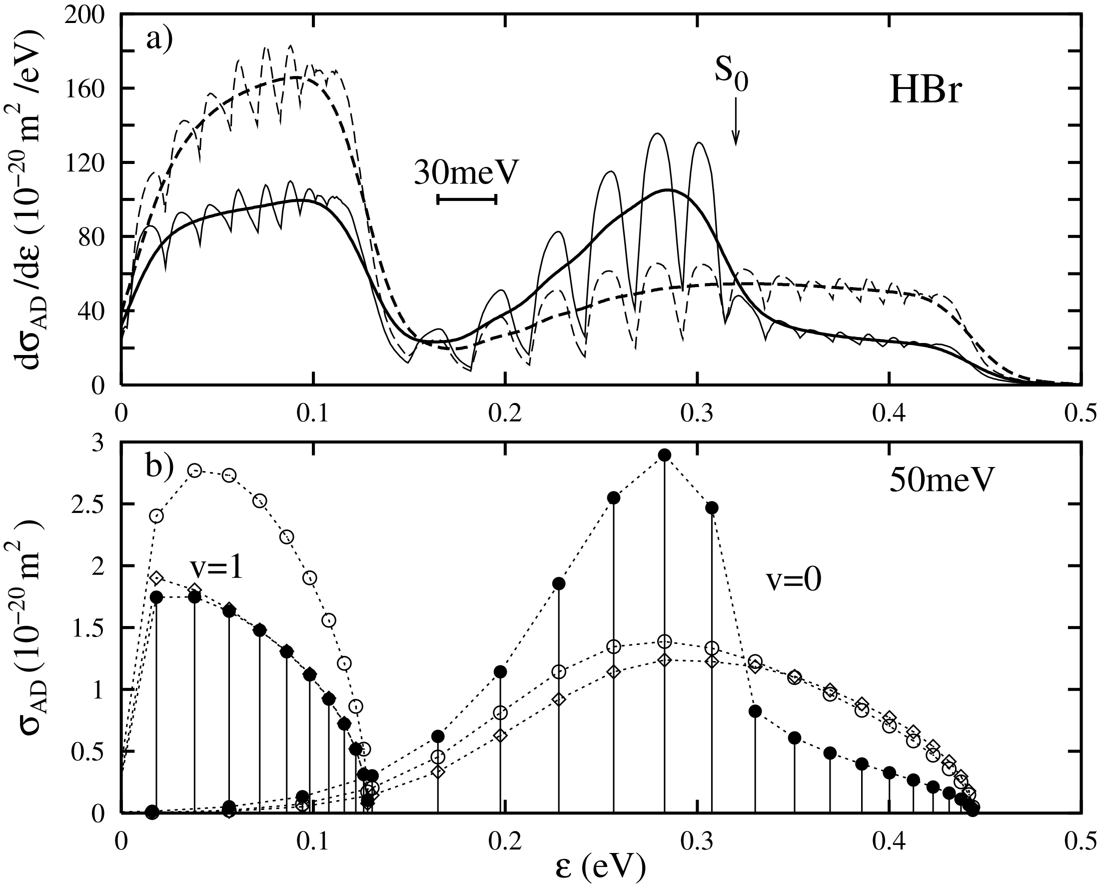

Figure 11. Results for associative detachment in H + Br^- collisions. **a)** Electron spectrum calculated for the collision energy distribution shown in figure 4, as obtained with a spectrometer width of 0 meV (thin line) and 30 meV (thick line). Results of the LCP calculation are shown with dashed lines. **b)** Cross sections $\sigma_{vJ}(E)$ for associative detachment versus electron energy $\varepsilon_{v,J}$ as calculated for the discrete collision energy 50 meV. The meaning of the symbols is the same as in figure 7.

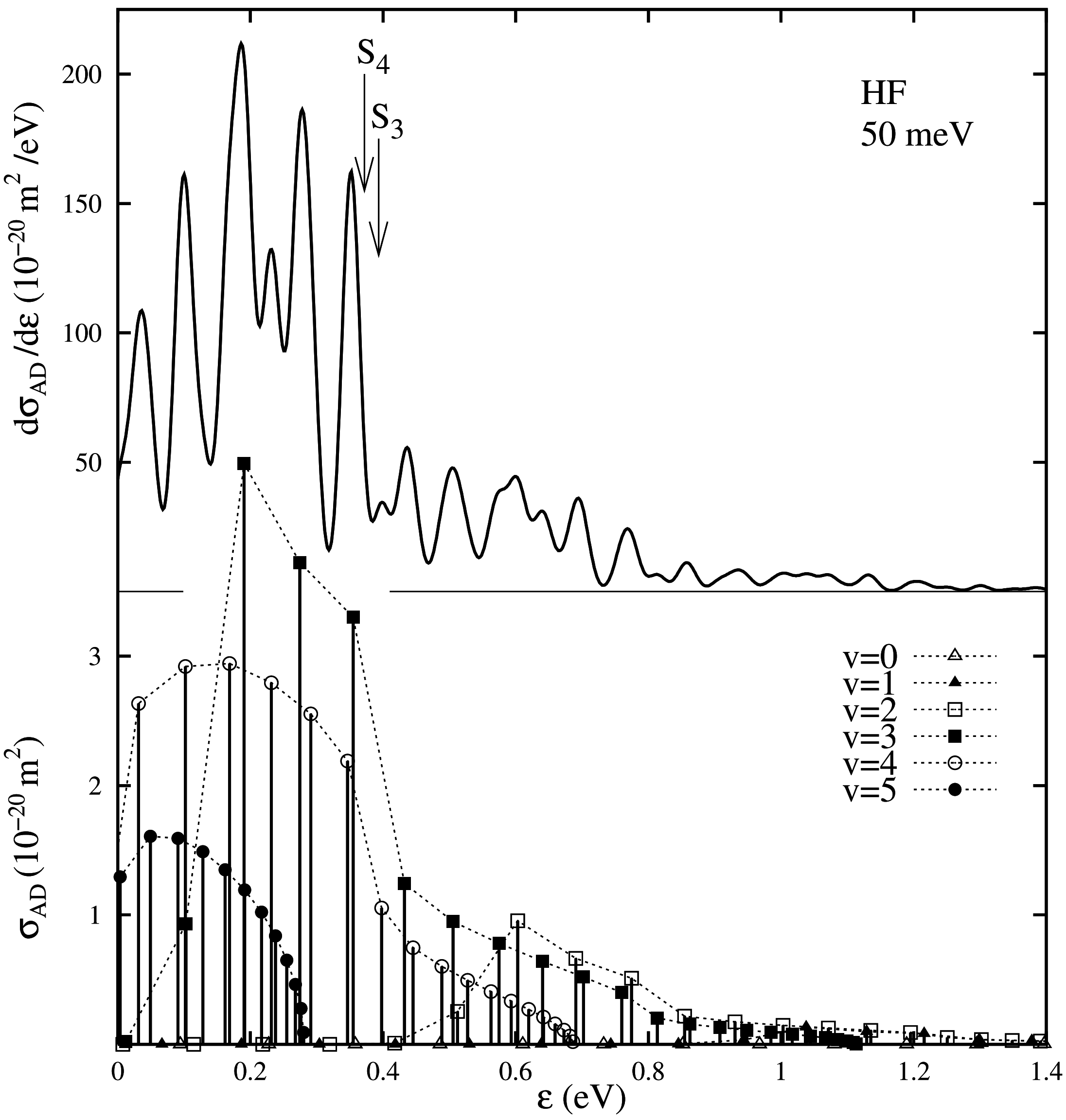

Figure 12. Cross sections $\sigma_{vJ}(E)$ for associative detachment in $H + F^-$ collisions versus electron energy $\varepsilon_{v,J}$, as calculated for the discrete collision energy 50 meV. The smooth curve (upper part) shows the corresponding simulated electron spectrum for the same collision energy and for a resolution of the electron spectrometer of 30 meV (FWHM). S_3 and S_4 denote the step-like increase of the rovibrational population in the nonlocal calculation for $v = 3$ and $v = 4$ associated with the closing of the $v = 4$ and $v = 5$ channel, respectively.